

Mineralization of Captured Per- and Polyfluoroalkyl Substances (PFAS) at Zero Net Cost Using Flash Joule Heating

Phelecia Scotland,^{1,2} Kevin M. Wyss,² Lucas Eddy,^{2,3,4} Yi Cheng,² Jacob L. Beckham,² Youngkun Chung,⁵ Bo Wang,⁵ Chi Hun Choi,^{1,2} Bing Deng,² Tengda Si,² Yu-Yi Shen,⁶ Sarah Grace Zetterholm,⁸ Christopher Griggs,⁸ Yimo Han,¹ Mason Tomson,⁶ Michael Wong,^{2,5} Boris I. Yakobson,^{1,2} Yufeng Zhao,^{*,1,9} and James M. Tour^{*,1,2,3,7}

¹Department of Materials Science and Nanoengineering, ²Department of Chemistry, ³Smalley-Curl Institute, ⁴Department of Applied Physics, ⁵Department of Chemical and Biomolecular Engineering, ⁶Department of Civil and Environmental Engineering, ⁷NanoCarbon Center, and Rice Adv. Mater. Institute, Rice University, 6100 Main Street, Houston, TX, 77005, ⁸U.S. Army Engineer Research & Development Center, Vicksburg, MS, 39180, USA. ⁹Corban University, 5000 Deer Park Drive SE, Salem, OR, 97317, USA.

*Corresponding Author Emails: yzhao@corban.edu; tour@rice.edu

Abstract Per- and polyfluorinated alkyl substances (PFAS) are persistent and widespread environmental contaminants that have infiltrated freshwater systems. Granular activated carbon (GAC), the most widely used sorbent for PFAS removal from water, becomes a secondary waste when PFAS is sorbed upon it (PFAS-GAC). Current methods for treatment of this contaminated spent carbon, such as incineration, release large amounts of hazardous gaseous fluorocarbons. To address these challenges, here we demonstrate the disposal of PFAS-GAC using an electrothermal

mineralization process. Flash Joule heating (FJH) of PFAS-GAC in the presence of sodium or calcium salts yields inert, non-toxic fluoride salts with >96% fluorine conversion efficiency. Simultaneously, the spent carbon is upcycled into high-value flash graphene, offsetting the cost of treatment by \$1900 US per tonne. The entire process operates without the need for solvents or expensive catalysts. The life cycle assessment (LCA) shows a reduction in cumulative energy consumption, greenhouse gas emissions, and water usage. The ease of scalability and the production of valuable co-products, as highlighted in the technoeconomic assessment (TEA), showcases this method as an attractive route to mineralize PFAS in ~1 s.

Keywords: PFAS, Flash Joule Heating, Upcycling, Fluoride, Mineralization.

1. Introduction

Per- and polyfluorinated alkyl substances (PFAS),¹ also commonly known as “forever chemicals”, refer to a group of synthetic compounds that have a combined market size of \$28 billion in 2023.² There are over 9,000 types of PFAS, all of them anthropogenic.¹ PFAS has been widely used in fire-fighting foams, CO₂-based dry cleaning, non-stick cooking surfaces, food containers, personal care products, and aqueous film-forming foams, making them pervasive in human society.^{3,4} Although they have many commercial applications, these once indispensable chemicals have recently been linked to several adverse health effects including cancer, immune suppression, and damage to the reproductive system, liver, kidney, and thyroid.^{5,6} Due to their chemical inertness, PFAS are not readily decomposed or expelled from the body.⁷ Now, these persistent, toxic compounds are ubiquitous in drinking water, soil, and the blood of humans and animals,^{8,9} posing an immediate threat to both health^{8–10} and the environment.^{11–14}

PFAS-contaminated water is a key source of exposure to the general population.^{14–16} In response to these concerns, the US Environmental Protection Agency (EPA) recently lowered the maximum contaminant level in drinking water of specific PFAS, including perfluorooctanoic acid (PFOA) and perfluorooctane sulfonic acid (PFOS), each from 70 ng/L to 4 ng/L.^{17,18} To comply with these stringent limits, several strategies have been employed to collect PFAS from water streams. A common strategy for mitigating PFAS accumulation in water is physiochemical adsorption. PFAS is adsorbed by granular activated carbon (GAC)^{16,19,20} via hydrophobic interactions and PFAS binds to anion exchange resins^{21,22} through ionic interactions. The chain length and functional groups of the PFAS substantially influence the efficiency of these techniques.

Although these sorbents are effective at removing PFAS, all sorption methods result in the production of secondary, now concentrated, sorbent wastes. These PFAS-laden sorbent secondary wastes are typically degraded through incineration,^{7,22–25} which requires temperatures of 1000 °C and long reaction times for complete PFAS degradation.²⁶ But, incomplete incineration can result in the formation of small, volatile organic fluorinated compounds (VOF) that are often more toxic than the starting PFAS.^{25,27,28} The EPA is considering banning the incineration of PFAS-containing materials due to the higher volatility and toxicity of these degradation products.²⁹

Here, we demonstrate a new strategy for the disposal of PFAS-laden GAC (PFAS-GAC) using flash Joule heating (FJH) to mineralize the sorbed PFAS. FJH is a process by which an electrothermal discharge is used to generate extremely high temperatures across resistive solid samples and thereby drive chemical decomposition (**Fig. S1**). We demonstrate that >96% of PFAS-GAC can be degraded during FJH, forming inorganic salts with <0.01% of the initial PFAS remaining. This is accomplished by the ≤ 1 s FJH of the PFAS-GAC in the presence of NaOH or Ca(OH)₂, achieving temperatures >2000 °C and mineralizing the organic fluorine to NaF or CaF₂, respectively. Furthermore, our results demonstrate that no detectable degraded VOF or short chain PFAS are formed in the FJH process in the presence of mineralizing reagents. The GAC is converted into crystalline flash graphene, a valuable co-product that can be sold to offset the cost of the decontamination process. The life cycle assessment (LCA) shows that this process offers low energy consumption and low water consumption, produces minimal greenhouse gas, while upcycling toxic and concentrated secondary waste streams into valuable graphene and inert inorganic salts.

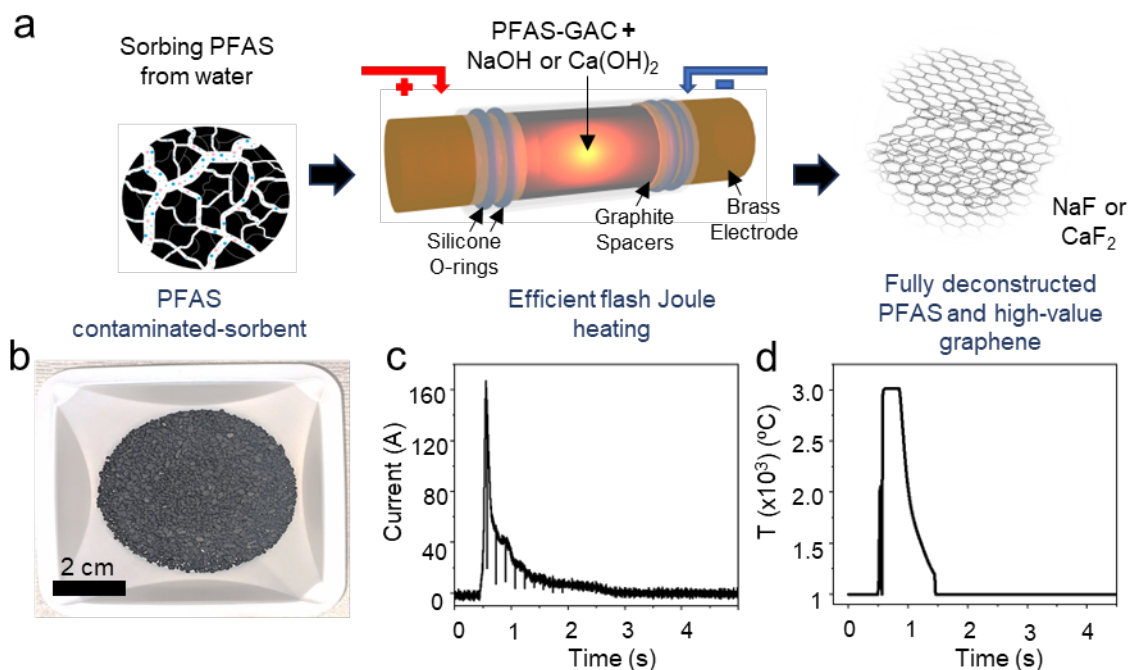


Fig. 1. Scheme, current and temperature of the FJH study. **a)** Schematic of the experimental setup and process. **b)** Image of PFOA-GAC in a weighing boat. **c)** Current profile of a typical 150 V (59 mF, 1.00-s FJH experiment) and **d)** the temperature profile of the FJH over the course of the reaction.

2. Results and Discussion

2.1 Direct Conversion of PFOA-GAC Into Inorganic Fluoride Salts by FJH

PFOA was used as a representative PFAS type. A mixture of PFOA-GAC and NaOH (see methods for more details) were packed into a quartz tube with double O-ring seals on each end, as illustrated in **Fig 1a**. The packed sample exhibited a typical resistance of 1.2 to 2.0 Ω , a suitable resistivity for direct-current FJH. **Fig. 1b** displays an image of the PFOA-GAC sorbent. The reactants were subjected to FJH at voltages from 110 to 150 V for durations of 0.50 and 1.00 s.

These reactions resulted in high current (**Fig. 1c**) and a rapid temperature increase up to $>3000\text{ }^{\circ}\text{C}$ (**Fig. 1d**) which decays over the course of 2 to 3 s.

While $\text{Ca}(\text{OH})_2$ is optimal for industrial use since the more common mineralized form of fluoride is as the calcium salt, we chose here to also use NaOH as the mineralizing reagent due to the higher solubility of NaF with water, facilitating easier quantification of the mineralization. The high temperatures achieved by the rapid resistive heating resulted in the reaction of PFOA with NaOH, forming NaF through the strong bond association of the fluoride anion to sodium cation (**Fig. S2**). The resulting products were analyzed using ion chromatography (IC) to quantify the degree of mineralization. **Fig. 2a** shows that an average of $\sim 96\%$ of organic F in PFOA was converted to inorganic fluoride at 130 V for 1.00 s when 1.2 mole equivalents (eq) of NaOH were used per mole of fluoride in the starting PFAS-GAC.

The sample mass, capacitance and voltage discharged through the sample directly determines the thermal energy generated and the highest temperature achieved. Reaction parameters of 150 V and 0.50 s duration yielded an average mineralization of 87% with a wide standard deviation. In contrast, using FJH at the same voltage but for a longer duration of 1.00 s resulted in 94% mineralization and a reduced standard deviation. Thus, longer reaction durations ensure that PFOA is further mineralized within the tube (**Fig 2a**).

We then studied the localization of NaF within the reaction vessel. **Fig. 2b-c** shows the recovery location for the resultant NaF within the reactor, as quantified by ion chromatography. Most of the inorganic salt was found mixed with the solid powder flash graphene product and deposited onto the graphite electrodes and some was deposited on the inner walls of the quartz tube.

High resolution X-ray photoelectron spectroscopy (XPS) in **Fig. 2d** compared the PFOA-GAC with the products from the FJH reaction at 150 V and 1.00 s. The F 1s peak of PFOA-GAC appears at a higher binding energy (688.9 eV) compared to that of the flashed product (684.5 eV). The corresponding F 1s peak of the product can be deconvoluted to a NaF peak at 684.5 eV and a second peak at 686.0 eV, indicating sodium fluorosilicate $\text{Na}_2(\text{SiF}_6)$. The $\text{Na}_2(\text{SiF}_6)$ is present in small amounts due to the reaction with the quartz tube. $\text{Na}_2(\text{SiF}_6)$ is water soluble, and the resultant anion can further dissociate into water to give fluoride ions.³⁰ Thus, the fluoride formed as $\text{Na}_2(\text{SiF}_6)$ is detected in the IC data.

Fluorine-19 nuclear magnetic resonance spectroscopy (^{19}F NMR) also shows the disappearance of the PFOA peaks and the formation of the same two types of inorganic fluoride detected by XPS (**Fig. 2e**). To determine if any PFOA remained on the flash graphene after the FJH reactions, the washed residual carbon samples were analyzed using LC-MS (**Fig. 2f**). The formation of any short-chain degradation products (C_2 to C_7) can similarly be observed by LC-MS. On average, <0.1% of PFOA remain when FJH reaction conditions are at 150 V and 1.00 s. The LC-MS and IC calibration curves are shown in **Fig. S3** and **Fig. S4-S5**, respectively. The concentrations of short-chain PFAS products (C_2 to C_7) fall below the instrumental detection limits when flashing at 130 V or 150 V for 1.00 s. This suggests that any short chain PFAS formed would be well-mineralized at higher voltages.

Gas chromatography-mass spectrometry (GC-MS) was used to ascertain whether VOF were being generated. Using a setup as described in **Fig. S6**, the off-gas from the reaction was captured and tested. GC-MS revealed a discernible trend: an increase in the stoichiometric ratio of NaOH corresponded to a decrease in the presence of evolved VOF (**Fig. 2g**). In the chromatogram, peaks 2.15 to 2.22 min corresponds to air. The peaks labeled 1, 2, 3 correspond to gases released

during the reactions and were identified as perfluoropentene, perfluorohexene, and perfluoroheptene, respectively. The mass spectra of these compounds are shown in **Fig. S6**. Importantly, the addition of 1.2 mol equivalents of NaOH per fluorine atom in a PFOA-GAC mixture resulted in a 99.81% mineralization of fluorine, as illustrated in **Fig. 2h** and **Table S1**, which approaches the limits of detection of our instrument. This result shows that the presence of excess mineralizing reagent can mitigate the formation of VOF in the degradation of PFAS-GAC.

During FJH, GAC was transformed into highly crystalline turbostratic flash graphene (GAC-FG). **Fig. 2i** illustrates the graphene yield for a representative set of samples obtained during the experimental process, affording >95% yield at 150 V for a 1.00 s flash. Additional spectroscopic and microscopic details regarding the produced graphene can be found in **Fig. S7-S14**.

The missing fluorine from the total mass balance was then investigated. The reaction tube post-FJH shows significant blackening especially near the middle section, furthest from the heat-sinking electrodes, where the reaction becomes hottest (**Fig. S15, S16**). After washing the tube and drying, Raman spectroscopy (**Fig. S17**) and XPS (**Fig. S18**) reveal peaks indicative of insoluble NaSiF₃O. The atomic percentage after rinsing ranges from 2.68% to 3.63% on the surface of the tube (**Table S2**). However, since XPS is a surface analytical method, it is difficult to quantitate this additional deposit of fluorine into a complete mass balance, but it is suggestive that the residual trace fluoride is not volatilized through the double-O-ring seals but reactive with the FJH vessel.

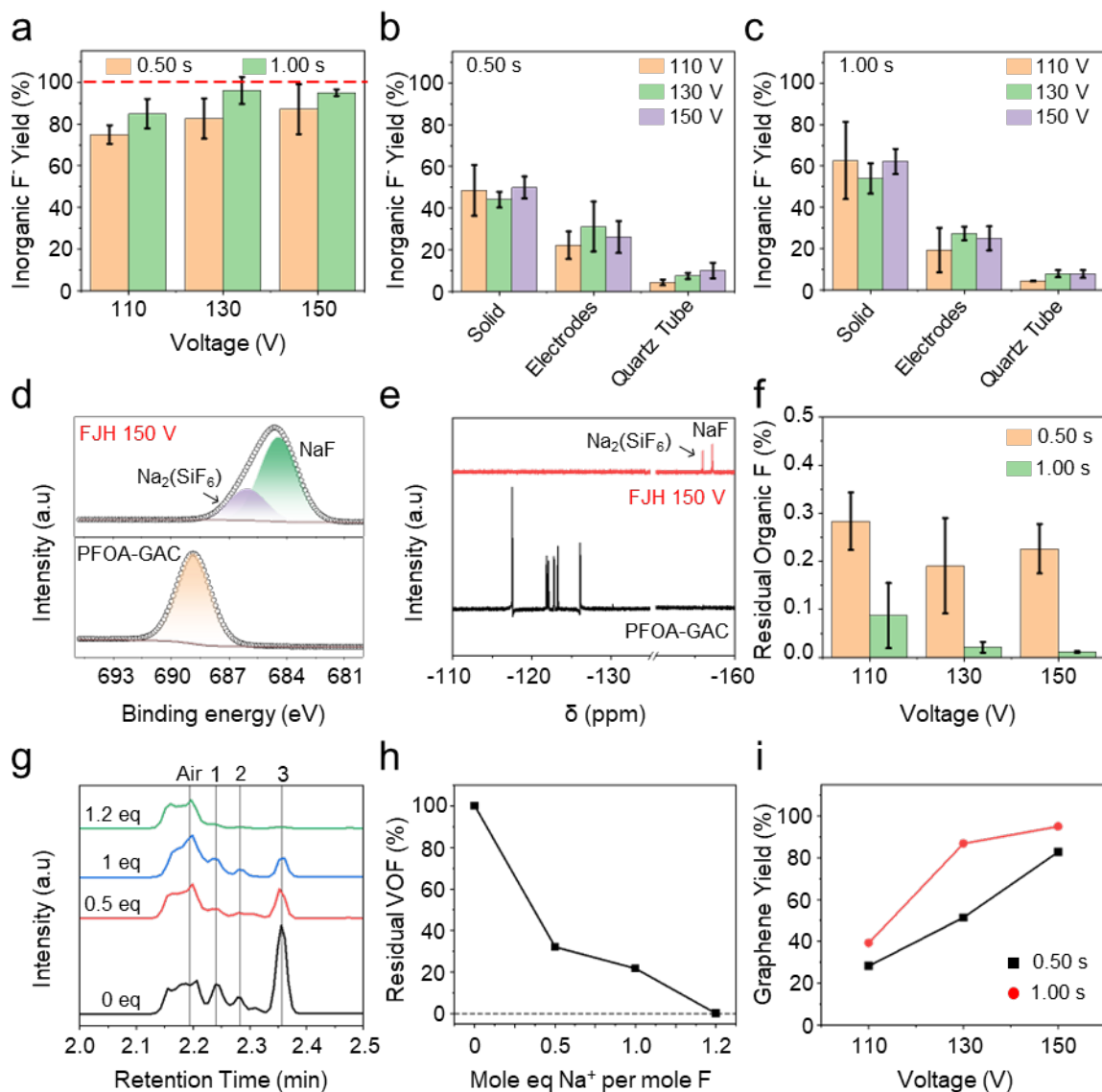


Fig. 2. Quantification and analysis of the mineralization process. **a)** Inorganic fluoride yield from FJH reaction of PFOA-GAC with 1.2 mole eq of sodium per mole of fluoride in PFOA ($n = 3$). **b-c)** The average mass yield distribution of the fluoride recovered from various parts of the reactor for different reaction conditions at 0.50 and 1.00 s flash durations, respectively ($n = 3$). **d)** High-resolution F1s spectra of the PFOA-GAC and fluoride salt/flash graphene product. **e)** ^{19}F NMR spectra of PFOA-GAC and flash graphene product. **f)** LC-MS analysis of residual organic fluorine recovered from the rinsed product ($n = 3$). **g)** GC-MS analysis of VOF produced during the reaction

using varying mole eq ratios of sodium per mole of fluoride in PFOA ($n = 1$). Peaks 1, 2, 3 correspond to the VOF evolved during the reactions and were identified as perfluoropentene, perfluorohexene, and perfluoroheptene, respectively. **h)** Remaining VOF with increasing mole eq of sodium per mole of fluoride ($n = 1$). **i)** Graphene yield for the FJH samples, showing representative graphene samples from the experimental process ($n = 1$). All error bars represent standard deviation.

2.2 Other PFAS-Sorbents and Mineralizing Reagents.

Other ionic salts can be used to promote the mineralization of fluorine. **Fig. S19** shows the efficacy of $\text{Ca}(\text{OH})_2$ as a mineralizing reagent. In keeping with the methodology employed for reactions using NaOH, PFOA-GAC was mixed with excess $\text{Ca}(\text{OH})_2$ (see methods) and subjected to FJH. The reaction at 150 V for 0.50 s resulted in 94% of the fluoride being converted into CaF_2 . Due to the insolubility of CaF_2 , the actual mineralization is likely higher. High quality graphene is also produced in high yield (**Fig. S19**). The inner surface of the reaction tube was analyzed using XPS (**Fig. S20**) after rinsing with 0.1 M of H_2SO_4 and drying. Up to 1.62% of surface fluoride can remain on the blackened area of the post-reaction tube (**Table S3**).

Alternative sorbents, such as anion exchange resins, offer an effective means of PFAS removal from water. One such example is Purofine PFA694 resin, consisting of polystyrene beads with amine-functional group, interacting through acid-base and hydrophobic forces. FJH of this PFAS-Resin is described in **Fig. S21**.

2.3 Molecular Dynamics Simulations

Optimized structures of PFOA and varying concentrations of NaOH were computationally heated at 1500 to 2500 K for 30 ps (**Fig. 3a**). Because the reaction leads to the cleavage of the C-F bonds in the PFAS, the number of C-F bonds in the system were used as a descriptor (**Fig. 3b**). Without any sodium salts, ~80% of the C-F bonds remained unbroken after annealing. For F to Na ratios of F₂₄₀Na₃₂, F₁₃₅Na₇₂, F₁₀₅Na₉₆ (in order of lowest to highest loading of Na), the amount of unbroken C-F bonds was 78%, 48%, and 15%, respectively. These reactions show that the ratio of unbroken bonds is substantially reduced with the addition of higher concentrations of sodium salts when annealed under similar conditions. Thus, sodium ions function as a catalyst that promotes the breakage of the C-F bond and enhances the rate of mineralization. Similar catalytic properties likely exist for other alkali metals and alkaline earth metals. **Fig. S22** shows the simulated and optimized structures for the lowest and intermediate loading of sodium salts.

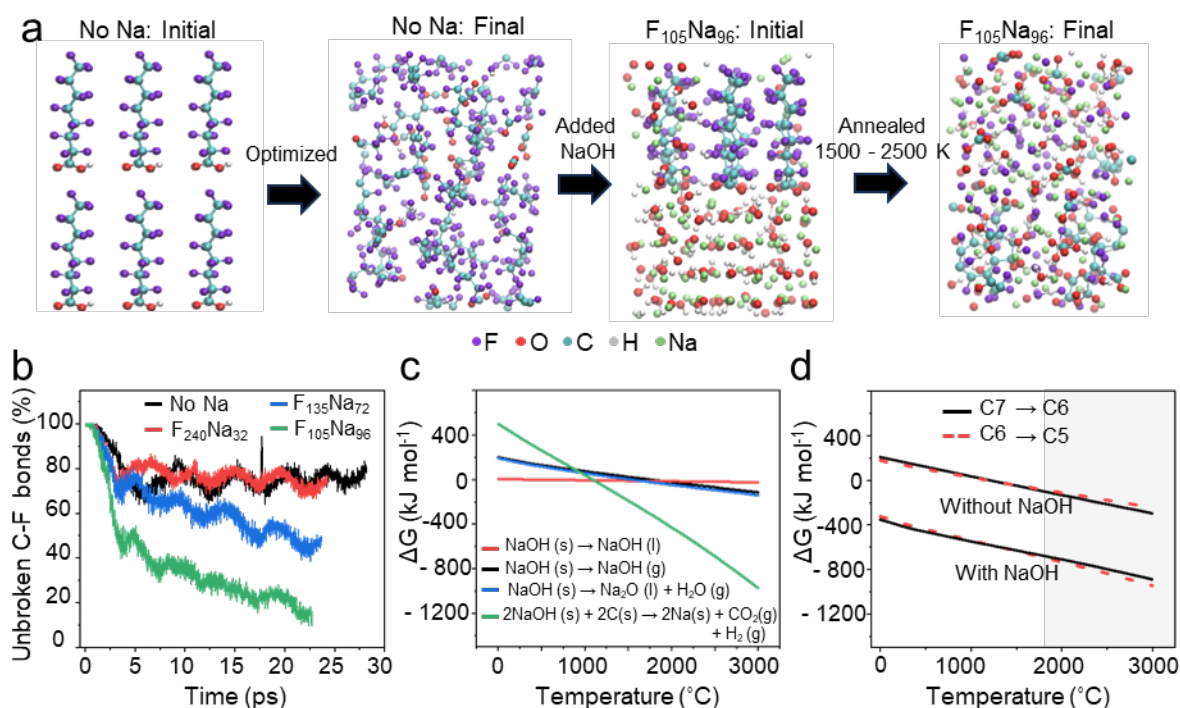


Fig. 3. Simulations of PFOA reacting with NaOH at high temperatures. **a)** Schematic of molecular dynamics simulation of optimized PFOA with the highest loading of NaOH (F₁₀₅Na₉₆), annealed

between 1500 and 2500 K. **b)** Number of unbroken C-F bonds calculated based on a). **c-d)** Thermodynamic analysis using the HSC chemistry package. **c)** The change in the Gibbs free energy suggests the most favorable reaction pathways for the NaOH mineralizing reagent during heating. **d)** The favorability of the reaction between fluorocarbons in the presence or absence of NaOH. The dark gray region represents average reaction temperatures.

2.4 Thermodynamic Analysis

Fig. 3c shows that melting of NaOH(s) into NaOH(l) is favorable when $T > 320$ °C. Therefore, it is likely that NaOH first melts, wetting the PFOA-loaded GAC and entering the porous carbon. This brings the mineralizing reagent into closer contact with the PFOA. The orange line in **Fig. 3c** represents the carbothermal reduction of NaOH during FJH conditions, forming Na metal when $T > 1140$ °C. This is an impetus for moving to the use of calcium salts such as Ca(OH)₂ or CaO when scaling up to minimize the accumulation of the more reactive Na(0). A precise mechanism for PFOA degradation via FJH is unknown. From the GC-MS result we observed that PFOA undergoes decarboxylation to form C₇F₁₆. During the reaction, C₇F₁₆ can break down into shorter chain species C₆F₁₄ and C₅F₁₂ by losing CF₂ and C₂F₄, respectively. **Fig. 3d** shows that these reactions are highly exothermic in the presence of NaOH due to the formation of NaF. This principle extends to the use of Ca(OH)₂ which forms the highly thermodynamically stable CaF₂ upon mineralization (**Fig. S2**).

2.5 Life Cycle Assessment (LCA) and Technoeconomic Assessment (TEA)

Due to the prevalent use of GAC to remove PFAS from wastewater, copious amounts of this contaminated carbon are generated, so a variety of disposal pathways are currently being

explored. To compare this FJH mineralization process to these other PFAS-GAC remediation methods, a comparative LCA was conducted. LCA is an analytical methodology used to examine the environmental impact of a product or process throughout its life cycle, from raw material extraction to disposal.^{31–33}

Here, five different PFAS-GAC disposal scenarios are compared: direct incineration,³⁴ ball milling assisted mineralization,³⁵ regeneration of GAC by microwave heating,¹⁹ solvent extraction,³⁶ and here mineralization by FJH. For regeneration methods of GAC remediation, the GAC can be reused, typically up to four times. Although we primarily used NaOH as the mineralizing reagent in FJH experiments to facilitate quantification of mineralized fluoride, we posit that in a scaled-up process, a calcium based mineralizing reagent would be used due to these reagents being more cost effective and without the generation of the more reactive sodium metal through carbothermic reduction during FJH. Furthermore, the inert and nontoxic byproduct, CaF₂, is more attractive since it is a natural mineralized form of fluoride in the environment, hence, the LCA and TEA were performed with Ca(OH)₂. The fate of the GAC, PFAS, and any required additives, for each method, are shown in **Fig. 4a**. Incineration and microwave GAC regeneration can release the fluorine from the PFAS in the form of CF₄ or other partially degraded organofluorines. These compounds, in addition to potentially being highly toxic, have remarkably high global warming potential, up to 7,000 times worse than CO₂ due to long atmospheric lifetime and UV adsorption.³⁷ **Fig. 4b** shows the cumulative energy demand for each process, demonstrating that compared to other methods, the FJH is highly efficient. **Fig. 4c** shows the global warming potential for each route. Due to the predicted production of CF₄ by microwave and incineration methods, since no mineralizing reagent is present, these methods have higher greenhouse gas emissions when compared to methods that mineralize fluoride. Incineration has

the lowest cumulative water usage followed closely by FJH (**Fig. 4d**). The production of the mineralizing reagent $\text{Ca}(\text{OH})_2$ is responsible for the difference in water usage. Considering the typical PFAS content on GAC is ≤ 1 wt % , the amount of CaF_2 generated in the flash graphene product is minimal. In most cases the non-toxic CaF_2 would not have to be removed especially if the product flash graphene is slated for use in concrete and asphalt which is the largest potential market for this material.³⁸ The full LCA breakdown is found in **Table S4-S8**.

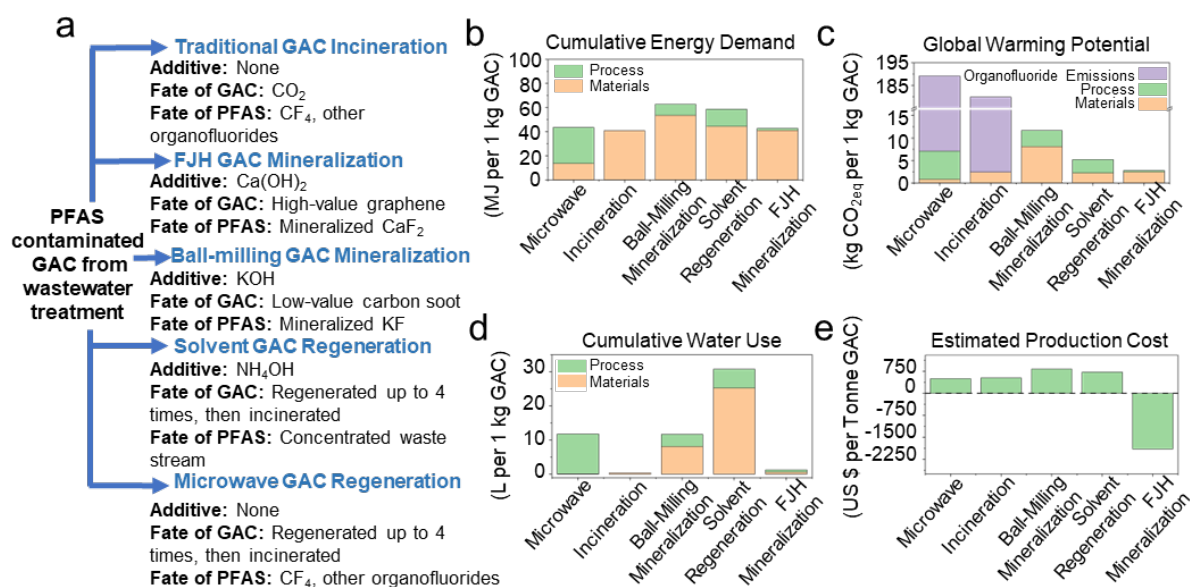


Fig. 4. Comparative LCA and TEA of FJH as compared to other PFAS-GAC remediation methods. **a)** Diagram showing the considered methods of PFAS-GAC remediation, with associated inputs and the fate of the GAC and PFAS. **b)** Cumulative energy demand of each GAC remediation method studied. **c)** Global warming potential of each GAC remediation method studied. **d)** Cumulative water use of each GAC remediation method studied. **e)** The projected cost of each process incorporates expenses related to both materials and the production process.

The TEA results are shown in **Fig. 4e**, illustrating the materials and process costs associated with scaling up these remediation methods to the 1-tonne scale. The materials cost is derived from the starting GAC and reagents (**Table S9-S10**). The process cost is based on the electrical consumption used in each method (**Table S11**). Notably, personnel and transportation costs were excluded from this analysis due to insufficient data in the literature. The starting material, GAC, can be transformed into valuable graphene, typically valued between \$60,000 to \$100,000 US per tonne.³⁹ Even considering a conservative worst-case scenario where graphene is sold at 5% of the low-end current cost, therefore sold at \$3,000 US per tonne, this process demonstrates the potential for a significant profit of ~\$1,900 US per tonne. **Fig. S23** shows the comparison of the five processes before the cost of graphene is considered. Taken together, these assessments underscore the prospect of FJH for mineralization of PFAS-laden sorbents.

3. Conclusion

This work demonstrates that the FJH process can rapidly degrade PFAS compounds while producing little or no harmful shorter-chain PFAS, VOF, or hydrogen fluoride. Though demonstrated here for the most common type of PFAS found in water, the FJH reaction temperatures of > 2000 °C will likely cause decomposition and mineralization of all PFAS types, when in the presence of sodium or calcium salts. Valuable graphene is produced as a product of this reaction, the sale of which can result in superior economic viability compared to other disposal methods that do not produce high value co-products. Instead of generating graphene, small modifications of the FJH process can alternatively afford carbon nanotubes, nanodiamonds or amorphous carbon, expanding the scope of the final carbon products.^{40,41}

4. Methods

4.1 Sample preparation

0.40 g of PFOA-GAC (39.48 mg of PFOA g⁻¹) was mixed with 69 mg of NaOH (1.2 mole eq of sodium per mole of F in PFOA). The sample was ground with mortar and pestle to ensure that the NaOH was in close contact with the to the PFOA. Then, 0.20 g of the mixture was mixed with 1.00 g of neat GAC and ground using a mortar and pestle providing a calculated starting concentration of 9.65 mg PFOA g⁻¹ sorbent. 0.10 g of that was subjected to FJH using a double O-ring sealed system (**Fig 1a**). The quartz tubes are prone to being shattered due to the pressure difference inside and outside of the tube. Thus, a spring wrapped outside the tube reduced the likelihood of tube shatter. The typical resistance across the sample in the quartz tube is 1.2 to 2.0 Ω . The current discharge is an unmodulated direct current (DC) discharge with a capacitance of ~59 mF, with the initial voltage and pulse time ranging from 110 to 150 V and 0.50 to 1.00 s.

0.40 g of PFOA-GAC (37.8 mg PFOA g⁻¹) was mixed with 61 mg of Ca(OH)₂ (1.2 mole eq of sodium per mole of F in PFOA) and ground using a mortar and pestle. 0.20 g of this mixture was mixed with 1.30 g of neat GAC. 0.10 g of this feedstock containing ~7.8 mg PFOA g⁻¹ of sorbent and was FJH at 110 to 150 V, 0.50 s and 59 mF. 0.1 M H₂SO₄ was used to rinse the post reaction samples to leach the CaF₂.

4.2 Characterization

The filtrates from the washing of the FJH products were analyzed for inorganic fluoride anions using ion chromatography on a Thermo Scientific Dionex Aquion. Chromatographic separation was achieved using the DionexTM IonPacTM AS23 IC Column 4×250 mm. The Mobile phase consists of 4.5 mM Na₂CO₃ and 0.8 mM NaHCO₃. The flow rate was 1 mL min⁻¹, and the column temperature was 30 °C. The resultant peaks were fitted between 4 and 5 min. We also

employed an alternative IC instrument when the Thermo Scientific Dionex Aquion was unavailable. The Metrohm 930 Compact IC Flex with column 4×250 mm. The eluent consisted of 3.2 mmol L⁻¹ Na₂CO₃ and 1.0 mmol L⁻¹ NaHCO₃, column temperature 25 °C, flow rate 0.700 mL min⁻¹, column pressure 11.83 MPa. The conductivity should be below 1.2 μS cm⁻¹ before the run. The fluoride peak was set at 6.10 min and the concentration was taken based on the area under the peak within a 5% window.

Two LC-MS instruments were used. The first was an Agilent 1290 Infinity Binary Pump LC coupled to an Agilent 6495C triple quadrupole MS/MS with Jet Streaming Technology and electrospray ionization (ESI). Chromatographic separation was performed using an Agilent Zorbax Eclipse Plus C18 column (2.1 × 100 mm, 1.8 μm). An Agilent Infinity Lab PFC Delay Column (4.6 × 30 mm) was used to delay any possible PFAS that is inherently in the system or mobile phases. The aqueous phase consisted of 2 mM ammonium acetate with 5% acetonitrile in MS-grade water (solvent A) and 100% MS-grade acetonitrile (solvent B). Chromatographic separation required a gradient elution with a flow rate of 0.35 mL min⁻¹. The analytical column was maintained at 40 °C throughout the run. The injection volume was 5 μL for this analysis. Data acquisition was performed in dynamic multiple reaction monitoring (dMRM) mode using negative-mode ESI.

The second LCMS instrument was the Agilent 1290 Infinity Binary Pump LC coupled to an Agilent 6470B triple quadrupole MS/MS through an Agilent Jet Spray (AJS) electrospray ionization (ESI) in negative ionization mode. Chromatographic separation was performed using an Agilent Zorbax Eclipse Plus C18 column (2.1 × 100 mm, 1.8 μm). An Agilent Infinity Lab PFC Delay Column (4.6 × 30 mm) was used to delay any possible PFAS that is inherently in the system or mobile phases. The injection volume of samples was 40 μL during the analysis. The aqueous

phase consisted of 20 mM ammonium acetate in MS-grade water (solvent A) and 100% MS-grade methanol (MeOH) (solvent B). Chromatographic separation required a gradient elution with a flow rate of 0.4 mL min⁻¹. The composition of mobile phase was ramped from 10% (solvent B) to 95% (solvent B) over 24 minutes and then held at 95% (solvent B) for 3 minutes. The analytical column was maintained at 40 °C throughout the run. The nebulizing gas (N₂) was set at a pressure of 35 psi during separation following voltage application. The source capillary voltage was set at 4000 V with the drying gas at a flow rate of 5 L/min and at a temperature of 230°C. For all PFAS standards, data acquisition was performed in dynamic multiple reaction monitoring (dMRM) mode under optimal fragmentation voltages.

An Agilent 8890 GC equipped with an Agilent HP-5ms low-bleed column (30 m, 0.25 mm internal diameter, 0.25 µm film) using He carrier gas for liquid and headspace sampling was used for GC-MS analysis. A tandem Agilent 5977B mass selective detector is used for liquid and headspace gas analysis.

Raman spectra were collected with a Renishaw Raman microscope using a 532 nm laser with a power of 5 mW. A 50× lens was used to collect all spectra. Analysis of Raman spectra, including peak intensity ratios, utilizes the height of the peak. Among these, 200 measurements were taken, and we only consider those with a discernable G peak. This avoids using unfocused measurements. Custom Python scripts⁴² were used to analyze Raman spectral mapping data by comparing peak intensity ratios and peak height. Graphene yield was calculated using I_{2D}/I_G ratios from these analyses. We looked for the I_{2D}/I_G > 0.3 then divided those ratios by the total number of spectra collected to give the graphene yield.

Powder XRD spectra were collected using a Rigaku SmartLab II using Powder XRD measurements were done on a Rigaku SmartLab Intelligent XRD system with filtered Cu Kα

radiation ($\lambda = 1.5406 \text{ \AA}$) zero background sample holders were used along at a scan rate of 5° min^{-1} and a 0.02° step size.

XPS data were collected using a PHI quantera SXM scanning X-ray microprobe with a base pressure of 5×10^{-9} Torr. Survey spectra were recorded using 0.5 eV step sizes with a pass energy of 140 eV. Elemental spectra were recorded using 0.1 eV step sizes with a pass energy of 26 eV. All the XPS spectra were corrected using the C 1s peaks (284.8 eV) as reference.

SEM images were taken with an FEI Helios Nanolab 660 Dual Beam SEM System. A voltage of 15 keV, a beam current of 100 pA, and a working distance of 4 mm were used for imaging. HR-TEM and HAADF-STEM images were taken with the FEI Titan Themis S/TEM instrument at 300 keV after accurate spherical aberration correction. Samples were prepared by drop-casting dilute F1DM/ethanol solutions onto lacey carbon grids.

The NMR spectra were taken using Bruker NEO 600 MHz High Performance Digital NMR with a helium cooled inverse TCI 600S3 H&F/C/N-D-05 ZXT probe. The sample temperature ranges from -40 to 150°C . The sensitivity of the probe based on the ^{19}F signal-to-noise ratio is 7000:1.

4.3 Materials

PFOA adsorbed onto GAC was obtained from the Army Corp of Engineers-ERDC, the GAC (Filtrisorb 400 or F400) was purchased from Chemviron Carbon. Activated charcoal used for solid-state dilution was obtained from MilliporeSigma (Product ID 242268-250G). Solid PFOA was obtained from SynQuest Laboratory. $\text{Ca}(\text{OH})_2$ was purchased from Fisher Scientific (C97-500). NaOH was obtained from MilliporeSigma (367176-2KG) and VWR Ion Chromatography (IC) PolyVials, 10571-344, from Avantor. F^- standard (1000 mg/L) was obtained

from MilliporeSigma (2121-3-18). Carbon black (CB, APS 10 nm, Black Pearls 2000) was purchased from Cabot Corporation.

4.4 Atomistic Modelling

Density Functional Theory (DFT) methods⁴³ are used as they are implemented in the Vienna Ab-initio Simulation Package (VASP).⁴⁴ A plane wave expansion up to 500 eV is employed in combination with an all-electron-like projector augmented wave (PAW) potential.⁴⁵ Exchange correlation is treated within the generalized gradient approximation (GGA) using the functional parameterized by Perdew-Burke-Ernserhof.⁴⁶ Because all the supercells are big enough with the smallest one being $15.0 \text{ \AA} \times 15.0 \text{ \AA} \times 22.0 \text{ \AA}$, only Γ point is used for the Brillouin zone integration over Monkhorst-Pack type mesh.⁴⁷ In structure optimization using the conjugate-gradient algorithm as implemented in VASP, both the positions of atoms and the unit cells are fully relaxed so that the maximum force on each atom is smaller than 0.01 eV \AA^{-1} . For modeling of catalytic reaction, the optimized structures are subsequently annealed for 30 ps with the temperature fluctuating at the range of 1500 - 2500 K in MD simulation. The MD simulation is performed using a Nose-Hoover thermostat and NVT ensemble with a time step of 0.5 fs. Because the catalytic reaction leads to the cleavage of the F-C bonds in the PFAS molecules, the number of C-F bonds were used in the system as a descriptor of the catalytic effect. The number of unbroken C-F bonds was calculated every 20 steps (10 fs) in each of the MD simulations and the results are shown in **Fig. 4 a-b**. In counting the number of C-F bonds, the cut-off distance is set at 1.55 \AA as compared to the equilibrium C-F bond length of 1.40 \AA .

5. Acknowledgement

The funding of the research is provided by Air Force Office of Scientific Research (FA9550-22-1-0526, J.M.T.), US Army Corps of Engineers, ERDC (W912HZ-21-2-0050, J.M.T., M.G.U.A., S.G.Z., C.G.), the National Science Foundation Graduate Research Fellowship Program (J.L.B.), the Stauffer-Rothwell Scholarship from Rice University (K.M.W.) and Rice Academy Fellowship (Y.C.). Permission to publish was granted by Director, Geotechnical & Structures Laboratory, ERDC. We acknowledge and thank Dr. Ashley Kimble and Mt. Justin Puhnaty from ERDC who contributed to the preparation of the PFOA-GAC used in this work. Dr. Bo Chen aided in the XPS analysis. The characterization equipment used in this project is partly from the Shared Equipment Authority (SEA) and the Electron Microscopy Core at Rice University.

6. Competing Interests

Intellectual property (IP) has been filed by Rice University on the FJH strategy for PFAS destruction which is being licensed to companies in which JMT is a shareholder, but not an officer, director or employee. Conflicts of interest are mitigated by disclosure to and compliance with the Office of Sponsored Programs and Research Compliance at Rice University.

7. References

1. Al Amin, Md., Sobhani, Z., Liu, Y., Dharmaraja, R., Chadalavada, S., Naidu, R., Chalker, J. M. & Fang, C. Recent Advances in the Analysis of Per- and Polyfluoroalkyl Substances (PFAS)—a review. *Environ. Technol. Innovation* **19**, 100879 (2020).
2. Glüge, J., Scheringer, M., Cousins, I. T., DeWitt, J. C., Goldenman, G., Herzke, D., Lohmann, R., Ng, C. A., Trier, X. & Wang, Z. An overview of the uses of per- and polyfluoroalkyl substances (PFAS). *Environ. Sci.: Processes Impacts* **22**, 2345–2373 (2020).

3. Hunter Anderson, R., Adamson, D. T. & Stroo, H. F. Partitioning of poly- and perfluoroalkyl substances from soil to groundwater within aqueous film-forming foam source zones. *J. Contam. Hydrol.* **220**, 59–65 (2019).
4. Xiao, X., Ulrich, B. A., Chen, B. & Higgins, C. P. Sorption of poly- and perfluoroalkyl substances (PFASs) relevant to aqueous film-forming foam (AFFF)-impacted groundwater by biochars and activated carbon. *Environ. Sci. Technol.* **51**, 6342–6351 (2017).
5. Stahl, T., Mattern, D. & Brunn, H. Toxicology of perfluorinated compounds. *Environ. Sci. Eur.* **23**, 38 (2011).
6. Sunderland, E. M., Hu, X. C., Dassuncao, C., Tokranov, A. K., Wagner, C. C. & Allen, J. G. A review of the pathways of human exposure to poly- and perfluoroalkyl substances (PFASs) and present understanding of health effects. *J. Exposure Sci. Environ. Epidemiol.* **29**, 131–147 (2018).
7. Sonmez Baghirzade, B., Zhang, Y., Reuther, J. F., Saleh, N. B., Venkatesan, A. K. & Apul, O. G. Thermal regeneration of spent granular activated carbon presents an opportunity to break the forever pfas cycle. *Environ. Sci. Technol.* **55**, 5608–5619 (2021).
8. Yeung, L. W., Miyake, Y., Taniyasu, S., Wang, Y., Yu, H., So, M. K., Jiang, G., Wu, Y., Li, J., Giesy, J. P., Yamashita, N. & Lam, P. K. Perfluorinated compounds and total and extractable organic fluorine in human blood samples from China. *Environ. Sci. Technol.* **42**, 8140–8145 (2008).
9. Aro, R., Eriksson, U., Kärrman, A. & Yeung, L. W. Organofluorine mass balance analysis of whole blood samples in relation to gender and age. *Environ. Sci. Technol.* **55**, 13142–13151 (2021).

10. Jia, X., Jin, Q., Fang, J., Shi, Y., Hou, M., Dong, H., Liu, Y., Deng, F., Zhou, Y., Godri Pollitt, K. J., Tang, S., Shi, X. & Cai, Y. Emerging and legacy per- and polyfluoroalkyl substances in an elderly population in Jinan, China: The exposure level, short-term variation, and intake assessment. *Environ. Sci. Technol.* **56**, 7905–7916 (2022).
11. Buck, R. C., Franklin, J., Berger, U., Conder, J. M., Cousins, I. T., de Voogt, P., Jensen, A. A., Kannan, K., Mabury, S. A. & van Leeuwen, S. P. Perfluoroalkyl and polyfluoroalkyl substances in the environment: Terminology, classification, and origins. *Integr. Environ. Assess. Manage.* **7**, 513–541 (2011).
12. Ellis, D. A., Mabury, S. A., Martin, J. W. & Muir, D. C. Thermolysis of fluoropolymers as a potential source of halogenated organic acids in the environment. *Nature* **412**, 321–324 (2001).
13. Brusseau, M. L., Anderson, R. H. & Guo, B. PFAS Concentrations in Soils: Background Levels Versus Contaminated Sites. *Sci. Total Environ.* **740**, 140017 (2020).
14. Scher, D. P., Kelly, J. E., Huset, C. A., Barry, K. M., Hoffbeck, R. W., Yingling, V. L. & Messing, R. B. Occurrence of perfluoroalkyl substances (PFAS) in garden produce at homes with a history of pfas-contaminated drinking water. *Chemosphere* **196**, 548–555 (2018).
15. Xiao, F., Hanson, R. A., Golovko, S. A., Golovko, M. Y. & Arnold, W. A. PFOA and PFOS are generated from zwitterionic and cationic precursor compounds during water disinfection with chlorine or ozone. *Environ. Sci. Technol. Lett.* **5**, 382–388 (2018).
16. McCleaf, P., Englund, S., Östlund, A., Lindegren, K., Wiberg, K. & Ahrens, L. Removal efficiency of multiple poly- and perfluoroalkyl substances (PFASs) in drinking water using granular activated carbon (GAC) and Anion Exchange (AE) column tests. *Water Res.* **120**, 77–87 (2017).

17. Belkouteb, N., Franke, V., McCleaf, P., Köhler, S. & Ahrens, L. Removal of per- and polyfluoroalkyl substances (PFASs) in a full-scale drinking water treatment plant: Long-term performance of granular activated carbon (GAC) and influence of flow-rate. *Water Res.* **182**, 115913 (2020).
18. Environmental Protection Agency. Per- and Polyfluoroalkyl Substances (PFAS) Proposed PFAS National Primary Drinking Water Regulation. (2023). [https://www.epa.gov/sdwa/and-polyfluoroalkyl-substances-pfas#:~:text=On%20March%2014%2C%202023%20%2C%20EPA,known%20as%20GenX%20Chemicals\)%2C%20perfluorohexane](https://www.epa.gov/sdwa/and-polyfluoroalkyl-substances-pfas#:~:text=On%20March%2014%2C%202023%20%2C%20EPA,known%20as%20GenX%20Chemicals)%2C%20perfluorohexane) accessed November 19, 2023.
19. Gagliano, E., Falciglia, P. P., Zaker, Y., Karanfil, T. & Roccaro, P. Microwave regeneration of granular activated carbon saturated with PFAS. *Water Res.* **198**, 117121 (2021).
20. Zhang, D., He, Q., Wang, M., Zhang, W. & Liang, Y. Sorption of perfluoroalkylated substances (PFASs) onto granular activated carbon and biochar. *Environ. Technol.* **42**, 1798–1809 (2019).
21. Chow, S. J., Croll, H. C., Ojeda, N., Klamerus, J., Capelle, R., Oppenheimer, J., Jacangelo, J. G., Schwab, K. J. & Prasse, C. Comparative investigation of PFAS adsorption onto activated carbon and anion exchange resins during long-term operation of a pilot Treatment Plant. *Water Res.* **226**, 119198 (2022).
22. Dastgheib, S. A., Mock, J., Ilangoan, T. & Patterson, C. Thermogravimetric studies for the incineration of an anion exchange resin laden with short- or long-chain PFAS compounds containing carboxylic or sulfonic acid functionalities in the presence or absence of calcium oxide. *Ind. Eng. Chem. Res.* **60**, 16961–16968 (2021).

23. Xiao, F., Sasi, P. C., Yao, B., Kubátová, A., Golovko, S. A., Golovko, M. Y. & Soli, D. Thermal stability and decomposition of perfluoroalkyl substances on spent granular activated carbon. *Environ. Sci. Technol. Lett.* **7**, 343–350 (2020).
24. Watanabe, N., Takata, M., Takemine, S. & Yamamoto, K. Thermal mineralization behavior of PFOA, PFHxA, and PFOS during reactivation of granular activated carbon (GAC) in Nitrogen Atmosphere. *Environ. Sci. Pollut. Res.* **25**, 7200–7205 (2018).
25. Watanabe, N., Takemine, S., Yamamoto, K., Haga, Y. & Takata, M. Residual organic fluorinated compounds from thermal treatment of PFOA, PFHxA and PFOS adsorbed onto granular activated carbon (GAC). *J. Mater. Cycles Waste Manage.* **18**, 625–630 (2016).
26. Stoiber, T., Evans, S. & Naidenko, O. V. Disposal of products and materials containing per- and polyfluoroalkyl substances (PFAS): A cyclical problem. *Chemosphere* **260**, 127659 (2020).
27. Feng, M., Qu, R., Wei, Z., Wang, L., Sun, P. & Wang, Z. Characterization of the thermolysis products of Nafion Membrane: A potential source of perfluorinated compounds in the environment. *Sci. Rep.* **5**, 9859 (2015).
28. Ellis, D. A., Martin, J. W., Muir, D. C. & Mabury, S. A. The use of ¹⁹F NMR and Mass Spectrometry for the elucidation of novel fluorinated acids and atmospheric fluoroacid precursors evolved in the thermolysis of fluoropolymers. *Analyst* **128**, 756 (2003).
29. DiStefano, R., Feliciano, T., Mimna, R. A., Redding, A. M. & Matthis, J. Thermal destruction of PFAS during full-scale reactivation of PFAS-laden granular activated carbon. *Rem. J.* **32**, 231–238 (2022).
30. Crosby, N. T. Equilibria of fluorosilicate solutions with special reference to the fluoridation of public water supplies. *J. Appl. Chem.* **19**, 100–102 (2007).

31. Finnveden, G., Hauschild, M. Z., Ekvall, T., Guinée, J., Heijungs, R., Hellweg, S., Koehler, A., Pennington, D. & Suh, S. Recent developments in life cycle assessment. *J. Environ. Manage.* **91**, 1–21 (2009).
32. Guinée, J. B., Heijungs, R., Huppes, G., Zamagni, A., Masoni, P., Buonamici, R., Ekvall, T. & Rydberg, T. Life cycle assessment: Past, present, and future. *Environ. Sci. Technol.* **45**, 90–96 (2011).
33. Hellweg, S. & Milà i Canals, L. Emerging approaches, challenges and opportunities in life cycle assessment. *Science* **344**, 1109–1113 (2014).
34. Chang, M. B. & Huang, C. K. Characteristics of energy flow in municipal solid waste incinerator. *J. Environ. Eng.* **127**, 78–81 (2001).
35. Zhang, K., Huang, J., Yu, G., Zhang, Q., Deng, S. & Wang, B. Destruction of perfluorooctane sulfonate (PFOS) and perfluorooctanoic acid (PFOA) by Ball Milling. *Environ. Sci. Technol.* **47**, 6471–6477 (2013).
36. Siriwardena, D. P., James, R., Dasu, K., Thorn, J., Iery, R. D., Pala, F., Schumitz, D., Eastwood, S. & Burkitt, N. Regeneration of per- and polyfluoroalkyl substance-laden granular activated carbon using a solvent based technology. *J. Environ. Manage.* **289**, 112439 (2021).
37. Tsai, W.-T. Environmental hazards and health risk of common liquid perfluoro-n-alkanes, potent greenhouse gases. *Environ. Int.* **35**, 418–424 (2009).
38. <https://www.universalmatter.com/> accessed November 29, 2023.
39. Wyss, K. M., Silva, K. J., Bets, K. V., Kittrell, C., Teng, C. H., Choi, C. H., Chen, W., Beckham, J. L., Yakobson, B. I., Tour, J. M. Synthesis of Clean Hydrogen Gas from Waste Plastic at Zero Net Cost. *Adv. Mater.* **35**, 2306763 (2023).

40. Wyss, K. M., Li, J. T., Advincula, P. A., Bets, K. V., Chen, W., Eddy, L., Silva, K. J., Beckham, J. L., Chen, J., Meng, W., Deng, B., Nagarajaiah, S., Yakobson, B. I. & Tour, J. M. Upcycling of waste plastic into hybrid carbon nanomaterials. *Adv. Mater.* **35**, 2209621 (2023).
41. Chen, W., Li, J. T., Wang, Z., Algozeeb, W. A., Luong, D. X., Kittrell, C., McHugh, E. A., Advincula, P. A., Wyss, K. M., Beckham, J. L., Stanford, M. G., Jiang, B. & Tour, J. M. Ultrafast and controllable phase evolution by Flash Joule Heating. *ACS Nano* **15**, 11158–11167 (2021).
42. Beckham, J. L., Wyss, K. M., Xie, Y., McHugh, E. A., Li, J. T., Advincula, P. A., Chen, W., Lin, J. & Tour, J. M. Machine learning guided synthesis of flash graphene. *Adv. Mater.* **34**, 2106506 (2022).
43. Dudarev, S. L., Botton, G. A., Savrasov, S. Y., Humphreys, C. J. & Sutton, A. P. Electron-energy-loss spectra and the structural stability of nickel oxide: an LSDA+U study. *Phys. Rev. B* **57**, 1505–1509 (1998).
44. Kresse, G. & Furthmüller, J. Efficient iterative schemes for *ab initio* total-energy calculations using a plane-wave basis set. *Phys. Rev. B* **54**, 11169–11186 (1996).
45. Blöchl, P. E. Projector augmented-wave method. *Phys. Rev. B* **50**, 17953–17979 (1994).
46. Perdew, J. P., Burke, K. & Ernzerhof, M. Generalized gradient approximation made simple. *Phys. Rev. Lett.* **77**, 3865–3868 (1996).
47. Monkhorst, H. J. & Pack, J. D. Special points for Brillouin-zone integrations. *Phys. Rev. B* **13**, 5188–5192 (1976).